International Journal of Concrete Structures and Materials

RESEARCH Open Access

Prediction of the R^3 Test-Based Reactivity of Supplementary Cementitious Materials: A Machine Learning Approach Utilizing Physical and Chemical Properties

Jinyoung Yoon[1*], Aidarus Yonis[2], Sungwoo Park[3], Farshad Rajabipour[4] and Sukhoon Pyo[2]

Abstract

This study utilized machine learning (ML) models to investigate the effect of physical and chemical properties on the reactivity of various supplementary cementitious materials (SCMs). Six SCMs, including ground granulated blast furnace slag (GGBFS), pulverized coal fly ash (FA), and ground bottom ash (BA), underwent thorough material characterization and reactivity tests, incorporating the modified strength activity index (ASTM C311) and the R^3 (ASTM C1897) tests. A data set comprising 46 entries, derived from both experimental results and literature sources, was employed to train ML models, specifically artificial neural network (ANN), support vector machine (SVM), and random forest (RF). The results demonstrated the robustness of the ANN model, achieving superior prediction accuracy with a testing mean absolute error (MAE) of 9.6%, outperforming SVM and RF models. The study classified SCMs into reactivity classes based on correlation analysis, establishes a comprehensive database linking material properties to reactivity, and identifies key input parameters for predictive modeling. While most SCMs exhibited consistent predictions across types, GGBFS displayed significant variations, prompting a recommendation for the inclusion of additional input parameters, such as fineness, to enhance predictive accuracy. This research provided valuable insights into predicting SCM reactivity, emphasizing the potential of ML models for informed material selection and optimization in concrete applications.

Keywords Artificial neural network, R^3 test, Modified strength activity index test, Material characterization

1 Introduction

The use of supplementary cementitious materials (SCMs) as a replacement for Portland cement offers significant benefits in terms of concrete production, encompassing durability, sustainability, and long-term strength development (Mehta and Monteiro 2013). Among various types of SCMs, fly ash (FA) and ground granulated blast furnace slag (GGBFS) have been mainly utilized due to their worldwide availability, cost-effectiveness, and eco-friendly attributes. However, with the retirement of coal power plants and the increasing adoption of electric arc furnace steel making systems over blast furnaces, concerns have been raised about the insufficient supply of these conventional

Journal information: ISSN 1976-0485 / eISSN 2234-1315.

*Correspondence:
Jinyoung Yoon
jyyoon@konkuk.ac.kr
[1] Department of Civil and Environmental Engineering, Konkuk University, Seoul 05029, Republic of Korea
[2] Department of Civil, Urban, Earth, and Environmental Engineering, Ulsan National Institute of Science and Technology, Ulsan 44919, Republic of Korea
[3] School of Architecture and Building Science, Chung-Ang University, Seoul 06974, Republic of Korea
[4] Department of Civil and Environmental Engineering, Pennsylvania State University, University Park, PA 16802, USA

Springer Open

© The Author(s) 2024. **Open Access** This article is licensed under a Creative Commons Attribution 4.0 International License, which permits use, sharing, adaptation, distribution and reproduction in any medium or format, as long as you give appropriate credit to the original author(s) and the source, provide a link to the Creative Commons licence, and indicate if changes were made. The images or other third party material in this article are included in the article's Creative Commons licence, unless indicated otherwise in a credit line to the material. If material is not included in the article's Creative Commons licence and your intended use is not permitted by statutory regulation or exceeds the permitted use, you will need to obtain permission directly from the copyright holder. To view a copy of this licence, visit http://creativecommons.org/licenses/by/4.0/.

SCMs to meet the demands of the concrete industry (Coal Combustion Products Production & Use Reports: ACAA 2019 CCP Survey Results 2019). As the SCM demand is expected to be growing, alternatives such as ground coal bottom ash (BA) (Kim 2015), calcined clay (CC) (Dhandapani et al. 2021; Jafari et al. 2022), fluidized bed combustion (FBC) ash (Yoon et al. 2022), and waste concrete powder (WC) (Vashistha et al. 2023), are being investigated. To enhance the utilization of various types of non-conventional SCMs, it is crucial to characterize their material properties and quantify their reactivities. Particularly, the correct identification and quantification of the reactivities of SCMs play an important role in their successful utilization in construction materials (ASTM C311/C311M-18, Standard Test Methods for Sampling and Testing Fly Ash or Natural Pozzolans for Use in Portland-Cement Concrete 2018).

One of the commonly used standardized methods for evaluating the reactivity of SCMs is through compressive strength test, such as those outlined in ASTM C311 (ASTM C311/C311M-18, Standard Test Methods for Sampling and Testing Fly Ash or Natural Pozzolans for Use in Portland-Cement Concrete 2018) and EN 196-5 (EN 196-5. Standard methods for testing cement. Part 5: Pozzolanicity test for pozzolanic cements 1988). For example, Strength Activity Index (SAI), as defined by ASTM C311 (ASTM C311/C311M-18, Standard Test Methods for Sampling and Testing Fly Ash or Natural Pozzolans for Use in Portland-Cement Concrete 2018), is determined by measuring the relative compressive strength of mortar samples where 20% of the Portland cement is replaced with SCMs, compared to a control mortar made with cement alone. In the SAI test, water-to-cement ratio (w/cm) is varied to achieve similar workability between the control and test mortars. The resulting difference in the w/cm, e.g., for SCMs having higher water requirement, can lead to a significant difference in the resulting strength development. To address this issue, some studies have assessed the reactivity at a constant w/cm; this is known as the modified SAI test (Wang et al. 2021). In case of modified SAI test, the addition of superplasticizers should be considered to maintain similar level of workability between control and test mortars (Kasaniya et al. 2022). A high SAI value is generally indicative of good reactivity in SCMs. However, the small replacement ratio of SCMs with cement and the influence of particle packing can lead to an inaccurate evaluation of the reactivity. Specifically, it has been reported that early age strength development is more influenced by the physical contribution, such as the filler effect of fine SCM particles (Kasaniya et al. 2022; Walker and Pavía 2011).

Alternatively, various test methods have been proposed to assess pozzolanic reactivity based on the consumption of calcium hydroxide (Chapelle 1958; Donatello et al. 2010; Tironi et al. 2013). The current standardized method for pozzolanic reactivity testing, as specified in EN196-5 and originating from the Frattini method (Frattini 1949), involves evaluating the concentration of Ca ions in a solution with cement and SCMs. The Chapelle test (Chapelle 1958) measures the consumption of portlandite in a mixture of cement and SCMs. While these test methods can assess the reactivity of SCMs by focusing on the changes in $Ca(OH)_2$, they may not be effective for SCMs with latent-hydraulic properties, such as GGBFS or high calcium FA (Li et al. 2018), limiting their applicability to specific SCM types.

In recent years, the Rapid, Relevant, and Reliable (R^3) test (ASTM C 1897) has been introduced to acquire reliable results regarding the reactivity of SCMs in terms of hydraulic and pozzolanic reaction within a 7-day period at an elevated temperature of 40 °C (ASTM C1897-20, Standard Test Methods for Measuring the Reactivity of Supplementary Cementitious Materials by Isothermal Calorimetry and Bound Water Measurements 2020). The R^3 test isolates the reaction of SCMs in simulated cement hydration environment, encompassing the presence of calcium hydroxide, calcite, sulfates, and alkalis. Results from the R^3 test, measuring the heat release and bound water after 7 days of reaction, exhibited strong agreement with chemical reactivity as determined by the strength tests (Avet et al. 2016; Li et al. 2018). Although initially developed for calcined clays and their blends with limestone, the R^3 test has proven to be reliable for various other SCMs, including FA, GGBFS, CC, natural Pozzolans, and their blends (de Azevedo Basto et al. 2023; Londono-Zuluaga et al. 2022; Parashar and Bishnoi 2020; Vayghan et al. 2021; Yoon et al. 2022). In addition, moderate or good correlations between characteristics of SCMs, such as particle size, chemical composition, and amorphous content, and their reactivity as obtained from the R^3 test were also found (Kasaniya et al. 2022; Yoon et al. 2022). However, one concern with the R^3 test lies in the necessity to measure cumulative heat release or bound water content at 3 and 7 days. To expedite the results of the R^3 test, a modified R^3 test, measuring heat release within 24 h, was also explored (Blotevogel et al. 2020). While the results indicated the effectiveness and reliability of the modified R^3 test for assessing the early age reactivity of GGBFS, it is essential to conduct further experimental work to validate this testing method for other SCMs.

Alternatively, the R^3-based reactivity of SCMs can be estimated based on their physical and chemical properties. However, the intricate relationship of reactivity

with the physical and chemical properties of SCMs has not been thoroughly investigated owing to their complex correlations and a limited number of available data. To address this, the use of machine learning (ML), known for its capacity to handle complex correlations and provide accurate predictions, can be considered, employing a comprehensive database for various SCMs. ML models have proven successful in solving regression problems in construction materials research, such as predicting concrete strength, durability, and slump (Li et al. 2022). Nevertheless, ML models have not been utilized for analyzing the R^3-based reactivity test considering various physical and chemical properties of SCMs.

The aim of this study is to develop the ML models for estimating the R^3-based reactivity of various SCMs based on their physical and chemical properties. First, a comprehensive investigation into the physical and chemical properties of SCMs belonging to GGBFS, FA, and BA groups and their reactivities assessed through both strength and R^3 tests was conducted. By integrating the experimental results with data from the literature, a comprehensive database including material properties and results from the R^3 test in terms of cumulative heat release was established. Using this database, several ML models, including artificial neural network (ANN), random forest (RF), and support vector machine (SVM), were developed. The performance of each ML model was assessed, and the prediction results based on materials properties were thoroughly analyzed.

2 Experimental Program

2.1 Materials

In this study, seven SCMs were investigated, categorized as follows: GGBFS, FA, and BA. GGBFS is an industrial by-product from a steel manufacturing industry and is a type of blast furnace slag obtained by water-quenching molten iron slag (Lee et al. 2019). Because of its rapid cooling process, GGBFS mainly consists of amorphous phase, generally resulting in excellent reactivity. FA and BA are by-products of coal-fuel thermal power plants, with FA typically constituting around 80% and BA around 20% of coal combustion by-products. The chemical composition of FA categorized it into Class F (CaO < 18%) and Class C FA (CaO > 18%) according to ASTM C618 (ASTM C618-19, Standard Specification for Coal Fly Ash and Raw or Calcined Natural Pozzolan for Use in Concrete 2019). Class F FA, commonly used as a pozzolanic material, is highly siliceous with a large quantity of amorphous phase. The median particle size of FA for use in concrete is approximately 10–15 μm, similar to that of most Portland cements. In contrast, BA has been disposed of in landfills due to its typically larger particle sizes (ranging from 0.1 mm to 20 mm) and highly porous structures (Yoon et al. 2019a). As a result, BA's use in concrete has been limited to use as lightweight aggregates. Using BA as SCM requires grinding to achieve a fine particle size (Kim et al. 2021; Pormmoon et al. 2021; Yoon et al. 2019a).

All SCMs used in this study included two samples of GGBFS labelled as GS1 and GS2, two BA samples labelled as BA1 and BA2, and two FA samples labelled as FA1 and FA2. All SCMs were collected from companies in South Korea. The as-received coarse BA samples were milled with a ball milling device for 24 h prior to use. The physical and chemical properties of the SCMs were investigated, as listed in Table 1. The characteristics of ordinary Portland cement used in the preparation of mortar samples for the strength test are also included in Table 1. Tests for physical properties encompassed particle size distribution (PSD), density, and moisture content. PSD was determined using laser diffraction with a Horiba LA-950. The density was identified according to ASTM C 188 (ASTM C188-17, Standard Test Method for Density of Hydraulic Cement 2017). Moisture content and the loss on ignition (LOI) of each SCM were measured by heating each sample to 110 °C and 750 °C, respectively, according to ASTM C311. Bulk chemical composition was quantified using fused bead X-ray fluorescence (XRF) spectroscopy.

The median particle sizes of BA1, and BA2, which underwent milling, were 79.5 μm and 66.0 μm, respectively; these were larger than the size of GGBFS and FA, and may lead to a lower reactivity. Similar chemical compositions were observed between GS1 and GS2, and between FA1 and FA2. BA1 showed similar chemical composition with FA1 and FA2, classifying BA1 as Class F according to ASTM C618 (ASTM C618-19, Standard Specification for Coal Fly Ash and Raw or Calcined Natural Pozzolan for Use in Concrete 2019). Conversely, BA2 contained a significant amount of CaO, exceeding 45%. BA2 was sourced from a thermal power plant using limestone for desulfurization during coal combustion, resulting in a higher percentage of CaO (and free lime) in the fly ash. According to ASTM C618 (ASTM C618-19, Standard Specification for Coal Fly Ash and Raw or Calcined Natural Pozzolan for Use in Concrete 2019), the moisture content of SCMs should be less than 3.0%. All SCMs met the requirement ranging from 0.1% to 2.0%. In terms of LOI, it is required to be less than 6.0%. All SCMs adhered to this requirement.

The mineralogy of each SCM was investigated through quantitative X-ray diffraction (XRD) analysis. Each SCM underwent grinding using a McCrone micronizing mill for 6 min to achieve a d50 of approximately 5 μm. The powdered sample was introduced into a back-loaded sample holder and placed on a spinner stage. A Malvern

Table 1 Physical and chemical properties of SCMs

		Portland cement	Granulated blast furnace slag		Fly ash		Bottom ash	
		CEM	GS1	GS2	FA1	FA2	BA1	BA2
XRF	CaO	64.2%	45.1%	43.6%	4.3%	4.2%	4.3%	45.1%
	SiO_2	19.1%	32.9%	33.0%	57.1%	62.7%	57.3%	32.9%
	Al_2O_3	4.6%	13.7%	14.4%	23.9%	22.5%	20.9%	13.7%
	MgO	2.1%	3.6%	4.1%	1.1%	1.0%	1.5%	3.6%
	SO_3	3.7%	1.9%	2.3%	0.6%	0.8%	0.3%	1.9%
	TiO_2	0.3%	0.8%	0.8%	1.4%	1.3%	1.4%	0.8%
	Fe_2O_3	3.6%	0.6%	0.5%	7.1%	4.2%	11.1%	0.6%
	K_2O	1.3%	0.6%	0.5%	1.4%	1.2%	1.5%	0.6%
	MnO	0.2%	0.4%	0.4%	0.1%	0.1%	0.1%	0.4%
	Na_2O	0.3%	0.3%	0.3%	1.7%	0.9%	0.7%	0.3%
$SiO_2 + Al_2O_3 + Fe_2O_3$		27.3%	47.2%	47.9%	88.1%	89.3%	89.3	47.2%
Particle size [μm]	D10	4.7	5.2	5.6	5.2	5.1	9.6	4.2
	D50	13.3	9.3	9.8	13.7	13.3	79.5	66.0
	D90	31.6	15.0	15.6	48.4	44.6	321.4	262.1
Density [g/cm^3]		3.11	2.89	2.87	2.22	2.29	2.45	2.85
Moisture content		0.1%	0.3%	0.2%	0.2%	0.5%	0.1%	0.3%
Free CaO		0.5%	0.1%	0.3%	0.2%	0.1%	0.0%	9.6%
Loss on ignition (LOI)		2.8%	0.0%	0.7%	2.8%	3.4%	2.0%	5.1%
Amorphous phase		–	98.5%	98.0%	66.2%	74.6%	75.2%	37.3%

Panalytical AERIS X-ray Diffraction equipment was used to conduct the XRD data acquisition. The incident X-ray beam from CuKa radiation was operated at 40 kV and 20 mA. Diffraction patterns were collected for approximately 30 min over the range of 8–70° 2-theta with a step size of 0.02°. For the quantification of individual mineral and amorphous phase, the Rietveld refinement was utilized using the external standard method (Scarlett and Madsen 2006; Singh et al. 2016). In the external standard method, the absolute weight fraction of each phase was calculated using the scale factors of phases and standard from the Rietveld refinement. The weight fraction (w_k) of a phase (k-phase) can be calculated as follows:

$$w_k = \frac{(ZMV)_k}{(ZMV)_s} \cdot \frac{S_k}{S_s} \cdot w_s \cdot \frac{\mu_m}{\mu_{ms}}, \quad (1)$$

where Z represents the number of formula units in the unit cell, M indicates the mass of unit cell, and V is volume of the unit cell. The $(ZMV)_k$ and $(ZMV)_s$ means constant values of the k-phase and the standard (labelled s), respectively. w_s is the crystallinity of the standard, S_k is scale factor of k-phase, S_s is scale factor of standard, μ_m is mass attenuation coefficient of bulk sample, and μ_{ms} is the mass attenuation coefficients of standard. Using Eq. (1), the weight fraction of each phase can be identified. Then, the weight fraction of amorphous phase can be obtained as follows:

$$w_{amorphous} = 1 - \sum_n w_n, \quad (2)$$

where $w_{amorphous}$ and w_n indicate weight fraction of amorphous and each phase. This quantification process was conducted using PANalytical X'pert HighScore Plus software (PANalytical X'Pert HighScore Plus 2012) and Inorganic Crystal Structure Database (ICSD 2012) (Inorganic Chemistry Structure Databases (ICSD) 2012). The crystalline products identified from the XRD analysis are illustrated in Fig. 1. The weight fraction of amorphous phase, related to the reaction of SCMs, is provided in Table 1.

GGBFS of GS1 and GS2 exhibited a large quantity of amorphous phase, exceeding 98%. Several peaks in GS1 and GS2 corresponded to C3S and akermanite. FA1 and FA2 samples displayed similar XRD patterns containing mullite, quartz, and magnetite. Amorphous phase contents for FA1 and FA2 were 66.2% and 74.6%, respectively. Considering the chemical composition of FA1 and FA2, they can be categorized as Class F according to ASTM C618 (ASTM C618-19, Standard Specification for Coal Fly Ash and Raw or Calcined Natural Pozzolan for Use in Concrete 2019). Regarding BA samples, it was found that XRD patterns for BA1 and BA2 had significant differences. The mineralogy and amorphous phase for BA1 was similar to FA1 and FA2. In contrast, BA2 had a

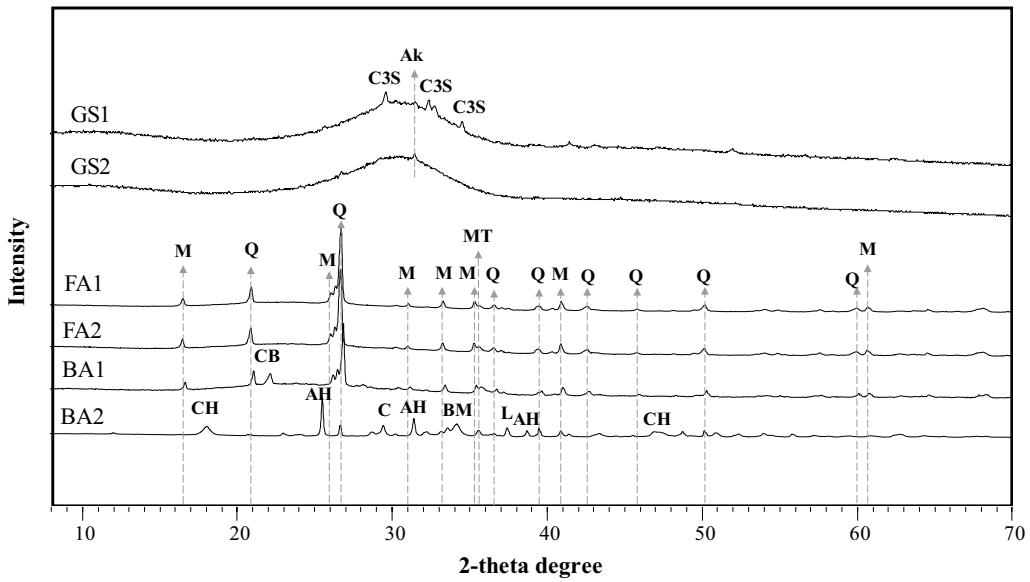

Fig. 1 Mineralogy of SCMs. *Ak* Akermanite, *C3S* 3CaO·SiO_2, *MT* magnetite, *M* mullite, *Q* quartz, *CB* cristobalite, *CH* portlandite, *AH* anhydrite, *L* lime, *C* calcite, *BM* brownmillerite)

relatively higher amount of CaO. Consequently, the mineralogy for BA2 included anhydrite, free lime and lime-weathering products, such as portlandite and calcite.

2.2 Methods for Evaluating the SCM Reactivity

2.2.1 Modified SAI Based on Compressive Strength Test

One of commonly used testing methods to assess the reactivity is based on the compressive strength test. The modified SAI was employed with reference to ASTM C311 (ASTM C311/C311M-18, Standard Test Methods for Sampling and Testing Fly Ash or Natural Pozzolans for Use in Portland-Cement Concrete 2018), with the exception that a constant w/cm of 0.49 was maintained for all mixtures. The replacement ratio of cement with SCMs was set at 20%. The cementitious materials-to-sand ratio was consistent at 2.75 for all samples. To measure the 7- and 28-day compressive strength, six-cube samples ($50\times50\times50$ mm^3) were made from each mix, with three samples utilized for measuring compressive strength at 7 and 28 days, each. Mortar sample were designated with a label in the format of M- followed by the name of SCM, such as M-GS1 for the mortar sample incorporating GS1.

2.2.2 Cumulative Heat Release and Bound Water Content from the R^3 Test

Another method employed for assessing the reactivity was the R^3 test, conducted in accordance with ASTM C1897 (ASTM C1897-20, Standard Test Methods for Measuring the Reactivity of Supplementary Cementitious Materials by Isothermal Calorimetry and Bound Water Measurements 2020). In this test, a lime-Pozzolan paste was prepared using 10 g of SCM, 30 g of $Ca(OH)_2$, 5 g of $CaCO_3$, and 54 g of alkaline solution consisting of 4 g of KOH and 20 g of K_2SO_4 dissolved in 1 L of deionized water. The pH of the solution was approximately 13.6 as specified in Sivakumar et al. (2021). For the R^3 test, the paste was mixed for 2 min at 1600 rpm, and then placed into 20 mL ampoules for an isothermal calorimeter test. During the first 7 days of hydration at 40 °C, the isothermal calorimeter measured the heat of hydration. The cumulative heat values per gram of SCM at 3 and 7 days were considered as indicators of SCM reactivity. In addition, chemically bound water in the R^3 paste at 3 and 7 days was measured. For this purpose, the paste was crushed and pieces smaller than 2 mm, totaling about 10 g, were placed in a crucible. The resulting specimen was dried in an oven at 105 °C for 2 h. Approximately 5 g of the dried specimen was heated at 350 °C for 2 h in an oven followed by cooling in a desiccator for 1 h over silica gel. The bound water of samples is equal to the mass loss between 40 °C and 350 °C divided by the mass of dried sample at 40 °C. (Avet et al. 2016). The weight loss between 105 °C and 350 °C is primarily due to dehydration of C–S–H.

2.3 Establishment of Database for Machine Learning-Based Models

In this study, seven SCMs were examined for their physical and chemical properties, as well as reactivity through

compressive strength and R^3 tests. To identify the intricate correlations between material properties and reactivity of SCMs, ML-based models should be developed. For the ML model training, data were collected from both experimental results obtained in this study and literature sources. A thorough literature review was conducted to collect information on properties and R^3 testing results of various SCMs. Given the recent standardization of the R^3 test, several studies have utilized this method to evaluate the reactivity of SCMs, including CC, volcanic ash (VA), FA, BA, fluidized bed combustion (FBC) ash, and GGBFS. A total of 12 papers featuring the R^3 test on SCMs was reviewed (Al-Shmaisani et al. 2022; de Azevedo Basto et al. 2023; Flegar et al. 2020; Kaladharan et al. 2023; Kasaniya et al. 2022; Li et al. 2018; Parashar et al. 2023; Sivakumar et al. 2021; Vayghan et al. 2021; Vladić Kancir and Serdar 2022; Weise et al. 2021; Yoon et al. 2022), but only five provided the necessary physical and chemical properties of SCMs along with the R^3 test results. By combining our experimental results with data from the literature review, a total of 46 data points for the ML model training was established, as shown in Fig. 2. It should be noted that all data used in this study are summarized in Table 6 in Appendix A.

2.4 Machine Learning-Based Models for Predicting the Reactivity

Various ML models were utilized here to predict reactivity of SCMs based on their material properties. Commonly employed ML models, including ANN, SVM, and RF models, which have been proven effective in analyzing construction materials (Li et al. 2022; Yoon et al. 2023; Yoon et al. 2019), were employed. To facilitate comparison, a linear regression (LR) model was also incorporated. This section presents an overview of the characteristics of ML and LR models.

2.4.1 Linear Regression (LR)

LR is a popular statistical method for estimating the output data based on independent input parameters. LR fits a linear regression between the multiple input and output variables using the ordinary least square method. A general form of LR is provided below:

$$Y = a_0 + \sum a_i X_i, \tag{3}$$

where Y is the output (i.e., R^3-based reactivity), X_i is the input variable (i.e., physical and chemical properties), and a_0 and a_i are the model coefficients. The optimization of model coefficients was carried out using the training data set, 80% of the database. Subsequently, the accuracy of the LR model was assessed using the testing data set. It should be noted that the identical training and testing data sets were utilized for all prediction models to facilitate meaningful comparisons.

2.4.2 Artificial Neural Network (ANN)

ANN serves as a mathematical modeling tool designed to analyze intricate relationships between input and output data by utilizing a network of highly interconnected neurons. The architecture of an ANN primarily comprises three layers: the input layer, hidden layer(s), and output layer (Eskandari-Naddaf and Kazemi 2017). The initial layer is the input layer, with the number of neurons corresponding to the number of input parameters. Upon the introduction of input data to the input layer, signals are transmitted to connected neurons in the hidden layers. Weighted signals from the hidden layers are further conveyed to the associated connected layer, known as the output layer. This process can be mathematically expressed as follows (Shiuly et al. 2022):

$$Y = f\left(\sum w_i x_i + b_i\right), \tag{4}$$

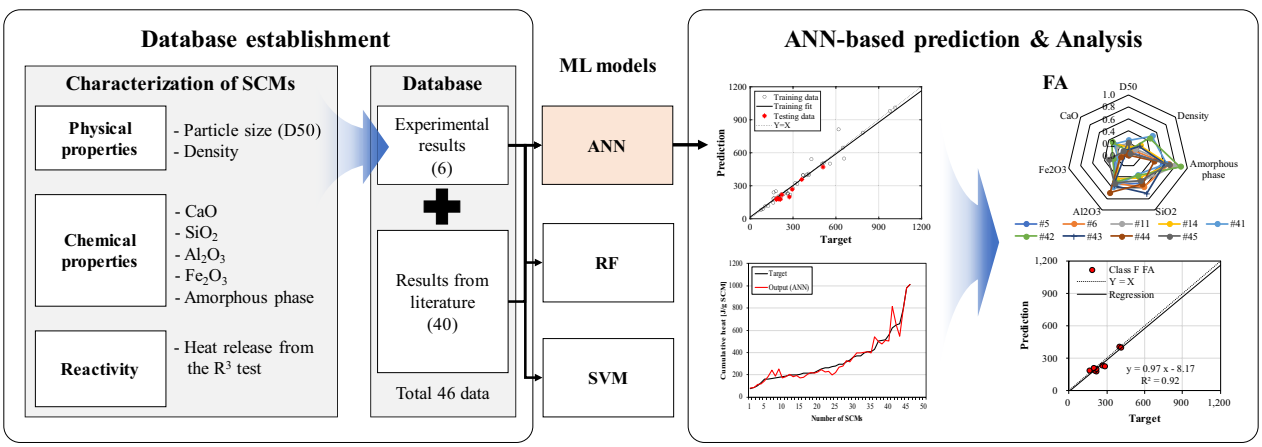

Fig. 2 Development of ML-based prediction model for R^3-based reactivity of SCMs using their physical and chemical properties

where w_i is the weight, b_i is the bias, and x_i is the input variable, and $f(x)$ is the activation function, and Y is the output value. The number of neurons in the output layer is equivalent to the number of output variables. It should be noted that in hidden layers, the quantity of neurons in each layer, as well as the number of hidden layers, can be adjusted based on the complexity of the relationship between input and output data. During the training of the ANN model, back-propagation is employed to fine-tune the weights and biases, aiming to minimize the mean square error (MSE) for predictions. The process continues until no further decrease in the MSE is observed. The optimal weights and biases for the ANN model are then selected to assess prediction accuracy using the testing data set.

2.4.3 Support Vector Machine (SVM)

The SVM has been used for classification and regression developed by Vapnik (Cortes and Vapnik 1995). Initially, the SVM was mainly used for classifications based on an optimal separation of classes by selecting a hyperplane with the maximum margin between classes. With the use of a ε-insensitive loss function, SVM can also address nonlinear regression problems (Yu et al. 2018). The original data set is transformed into a higher dimensional space through a kernel function, allowing SVM regression to operate in the feature space using a kernel function. The accuracy of SVM regression is influenced by the kernel functions (e.g., Gaussian and polynomial kernel). Due to the global optimization properties inherent in SVM regression, it can mitigate overfitting issues. In the present study, the Gaussian kernel function was selected, taking into account the nonlinearity of both input and output variables:

$$f(x) = \sum w_k h_k(x) + b, \tag{5}$$

where h_k means the nonlinear mapping function, w_k denotes the connection weight vector, and b indicates the bias. The optimization for coefficients can be obtained by solving minimization with objective function. Details for SVM regression model are also specified in Yu et al. (2018):

$$R_{\text{obj}}(C) = \frac{C}{m} \sum H[y_k, f(x_k)] + \frac{1}{2}\|w\|^2. \tag{6}$$

2.4.4 Random Forest (RF)

The RF algorithm is a composite of multiple trees, with each decision tree constructed using a training data set from the original training data through the bagging method (Breiman 2001; Han et al. 2019). When applied to regression problems, the RF model fits the output variables using samples of the input parameters. For each input variable, data are partitioned at various points, and the MSE is computed at each division point. The node is then assigned the minimum MSE value. In addition, the significance of variables can be gauged by permuting the values of input variables and observing the changes in prediction accuracy in out-of-bag samples. The RF model provides insights into the importance and impact of each input parameter on prediction outcomes. The underlying principle involves assessing the influence of an input variable, x_j, on prediction by evaluating changes in MSE. The model's prediction accuracy may decrease when the values of variable x_j are permuted. Consequently, variables are individually permuted, and the resulting reduction in prediction accuracy is measured. A greater decrease in prediction accuracy indicates a stronger association between the permuted variable and the response. For feature importance analysis, permutation-based MSE reduction is utilized. The equation for feature importance can be expressed as follows (Han et al. 2019):

$$\text{Feature importance}(x_j) = \frac{\text{MSE}\left(T_{D(\theta_i)}\right) - \text{MSE}\left(T_{D^j_{\text{OOB}}(\theta_i)}\right)}{\frac{1}{K}\sum_{i=1}^{K}\left(\text{MSE}\left(T_{D(\theta_i)}\right) - \text{MSE}\left(T_{D^j_{\text{OOB}}(\theta_i)}\right)\right)}, \tag{7}$$

where $T_{D(\theta_i)}$ is the ith tree predictor with $D(\theta_i)$ indicating bagged samples in ith tree. $D^j_{\text{OOB}}(\theta_i)$ represents permuted variable x_j in the out-of-bag (OOB) samples in $D(\theta_i)$. K means number of tree predictors in the forest.

2.4.5 Evaluation of Model Performance

The performance of ML-based models, namely ANN, RF, and SVM, was evaluated by comparing the accuracies of the actual and predicted values. Three statistical criteria of correlation coefficient (r), root mean square error (RMSE), and mean absolute error (MAE) were utilized for this evaluation. The r value indicated the linear correlation between the actual and predicted values, providing insight into the strength and direction of the relationship. To gauge the average error, two metrics of RMSE and MAE were utilized. RMSE calculates the square root of the average squared differences between actual and predicted values, offering measure of the overall accuracy. On the other hand, MAE computes the average absolute differences between target and prediction, providing a robust indicator of prediction accuracy. The following equations were used to determine each parameter:

$$r = \frac{\sum (x - x\prime)(y - y')}{\sqrt{\sum (x - x')^2 \sum (y - y')^2}}. \tag{8}$$

$$\mathrm{RMSE} = \sqrt{\frac{1}{n}\sum (y - y')^2}. \tag{9}$$

$$\mathrm{MAE}(\%) = \frac{1}{n}\sum \frac{|y - y'|}{|y'|} \times 100. \tag{10}$$

3 Experimental Results

3.1 Results of Modified SAI Test

Compressive strength of mortar samples, using mixture proportions outlined in Sect. 2.2.1, was evaluated after curing for 7 and 28 days, as shown in Fig. 3. At 7 days, M-GS2 exhibited the highest compressive strength, reaching 40.3 MPa. M-GS1, M-BA1, and M-BA2 showed a comparable 7-day compressive strength, ranging from 28.0 to 34.6 MPa. Meanwhile, the compressive strength of M-BA2, M-FA1, and M-FA2 was approximately 23.0 MPa at 7 days. At 28 days, a significant enhancement in compressive strength was observed for M-GS1 from 28.2 MPa at 7 days to 51.4 MPa. Because of the similar chemical and physical composition of GS1 and GS2, both M-GS1 and M-GS2 demonstrated a comparable level of compressive strength exceeding 50 MPa, indicating the high reactivity of GS series as SCMs. Samples, such as M-BA1, M-BA2, M-FA1, and M-FA2, showed compressive strength ranging from 31.1 to 37.7 MPa at 28 days. The strength test confirmed that highly reactive GGBFS, such as GS1 and GS2, contributed significantly to the development of compressive strength at 28 days. In can be concluded that GS1 is a highly reactive SCM, as expected.

The relative strength in Fig. 3 was determined by calculating the ratio of the compressive strength of SCMs-incorporated samples to the control sample. At 7 days, relative strength was mostly below 100%, except for M-GS2. At 28 days, both M-GS1 and M-GS2 exhibited relative strength of 113.4% and 123.3%, respectively. These results indicate that GS series possessed good reactivity, suggesting that a 20% replacement of cement with GS can maintain the compressive strength of the control sample at 28 days. The relative strength of FA and BA series at 28 days ranged from 68.5% to 83.1%, indicating moderate reactivity.

3.2 Cumulative Heat Release and Bound Water from the R^3 Test

The R^3 test for all SCMs measured cumulative heat release and bound water content for 7 days to evaluate the reactivity. The results of cumulative heat release of the R^3 paste incorporating SCMs are presented in Table 2 and Fig. 4. The highest heat release, reaching 657.3 J/g of SCM, was observed for GS2, attributed to the reaction of large amount of amorphous silica and $Ca(OH)_2$ in the R^3 environment (Al-Shmaisani et al. 2022). Similarly, GS1 also exhibited a significant heat release. FA1, FA2, and BA1 showed a heat release of approximately 200 J/g of SCM at 168 h. In contrast, R^3 pastes

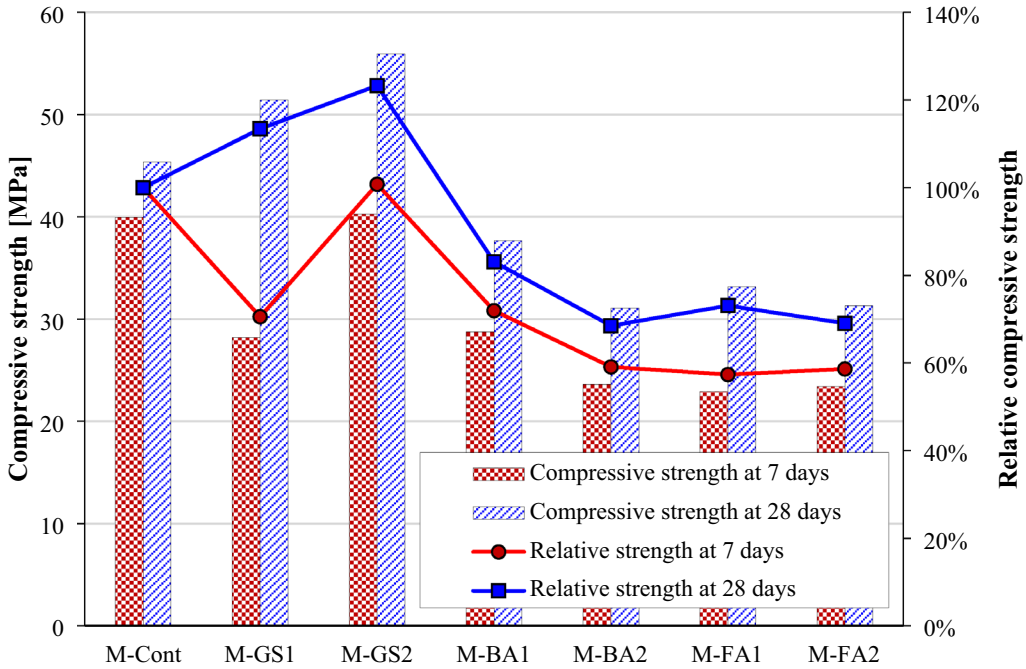

Fig. 3 Compressive strength and relative strength of mortar samples obtained from the modified SAI test

Table 2 Results of cumulative heat release and bound water obtained from the R^3 test

	Cumulative heat release (J/g of SCM)		Bound water (g/100 g of dried paste)	
	3 days	7 days	3 days	7 days
R3-GS1	396.4	428.8	18.0	32.0
R3-GS2	499.2	657.3	14.0	36.0
R3-BA1	97.4	216.5	13.0	15.0
R3-BA2	66.2	76.0	4.0	5.0
R3-FA1	132.1	212.4	5.0	8.0
R3-FA2	118.0	199.8	8.0	9.0

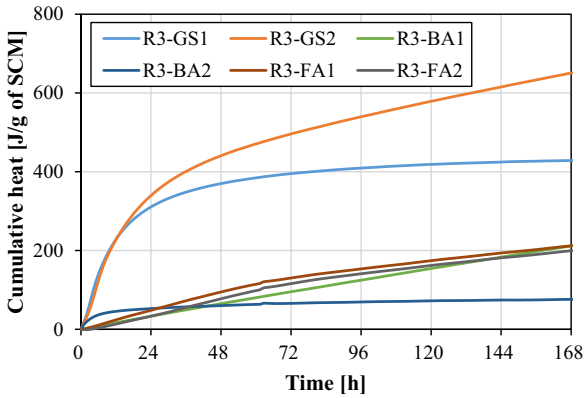

Fig. 4 Heat release of R^3 pastes for 7 days

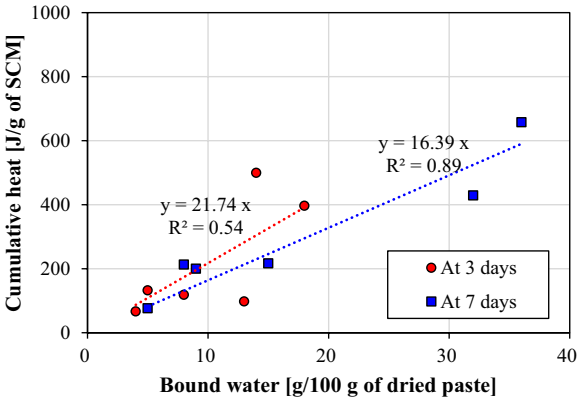

Fig. 5 Correlation of cumulative heat and bound water at 3 and 7 days obtained from the R^3 test

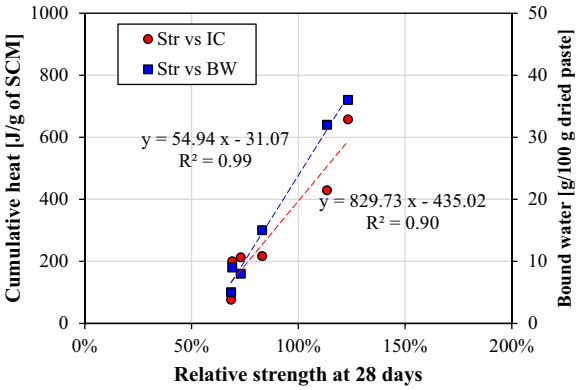

Fig. 6 Relationship of relative strength (Str) with the cumulative heat from the isothermal calorimeter test (IC) and bound water (BW) obtained by the R^3 test

incorporating BA2 displayed lower heat release of 76 J/g of SCM, respectively.

High cumulative heat release in the R^3 paste corresponds to an increased bound water content due to the generation of hydration products. Fig. 5 illustrates linear correlations between cumulative heat release and chemically bound water content. At 3 days, a moderate linear relationship was found with an R^2 of 0.54. Meanwhile, a stronger agreement between cumulative heat and bound water was observed at 7 days, showing an R^2 of 0.89. Based on the R^3 test results, GS1 and GS2 can be classified as highly reactive materials, while BA and FA samples can be considered moderately reactive materials.

The results of the R^3 test, including cumulative heat release and bound water content at 7 days, were compared to the relative strength, as depicted in Fig. 6. Relationships between relative strength, cumulative heat, and bound water content exhibited good correlations ($R^2 > 0.90$). These findings indicate that the R^3 test can effectively assess the reactivity of SCMs by isolating their reaction in a simulated cement hydration environment while excluding the particle packing effect. Therefore, estimating the cumulative heat or chemically bound water of SCMs from the R^3 test serves as a crucial parameter for comprehending and characterizing the chemical reactivity within a cementitious environment. This estimation can be enhanced by employing a ML-based model, incorporating both physical and chemical properties of SCMs.

4 Database Establishment Based on a Comparative Analysis

To develop a reliable and robust ML-based prediction model for assessing the reactivity of SCMs, it is important to establish a comprehensive quality database. Based on literature review (Al-Shmaisani et al. 2022; Avet et al. 2022; de Azevedo Basto et al. 2023; Vayghan et al. 2021; Yoon et al. 2022), a total of 40 data set was collected, and combined with our experimental results of six data sets. The database encompasses various types of SCMs, including 9 FA, 5 GGBFS, 6 BA, 3 metakaolins, 5 CC, and other SCMs, such as volcanic ash, FBC ash, and blended SCMs. Each data set contained parameters, such as mean particle size (D50), specific gravity, amount

of chemical composition (e.g., SiO_2, Al_2O_3, Fe_2O_3, and CaO) from XRF, and amorphous phase content quantified by XRD analysis, and reactivity based on cumulative heat at 7 days from the R^3 test. All data used in this study are provided in Appendix A, and their minimum, maximum, average, and standard deviation are summarized in Table 3. Given the impact of particle size, density, chemical composition and amorphous phase on the chemical reactivities of SCMs evaluated by the R^3 test (Londono-Zuluaga et al. 2022; Wang 2023; Yoon et al. 2022), input and output parameters were defined as shown in Table 3.

Due to the diverse requirements for SCM properties and the limited availability of data, it is necessary to acknowledge the restricted number of available data sets. Moreover, it is noteworthy that many previous studies have preferred to evaluate SCM reactivity using the heat release rather than bound water content from the R^3 test. This might be attributed to relatively larger interlaboratory variations observed in the bound water results due to sensitivity issues (Londono-Zuluaga et al., 2022). Thus, this study also utilized cumulative heat release value at 7 days from the R^3 test for the ML model development. For the training and testing phases of the ML models, the database was randomly divided into training (80%) and testing (20%) data sets. This approach ensures a robust evaluation of the developed ML models and enhances their predictive capability.

Fig. 7 illustrates the correlations between material properties and cumulative heat release. A moderate linear correlation between Al_2O_3 content and heat release is observed in Fig. 7f. This is associated with the higher evolution of heat during the hydration reaction of SCMs containing increased aluminate phases (Parashar et al. 2023). It can be inferred that the reaction products of aluminate-rich SCMs in the R^3 environment may encompass ettringite, monosulfates, hemicarbonates, and monocarbonates, as identified by XRD analysis in previous studies (Parashar et al. 2023; Yoon et al. 2022). However, except for Al_2O_3 content, no distinct correlations were evident between the properties of SCMs and cumulative heat at 7 days. This indicates the existence of a complex relationship between material properties and chemical reaction of SCMs.

Table 3 Summary of the database

		Min	Max	Average	Standard deviation
Inputs	Particle size (D50) (μm)	2.2	79.5	16.0	14.7
	Density (g/cm^3)	2.10	3.66	2.60	0.31
	CaO	0%	45.1%	10.8%	13.5%
	SiO_2	21.3%	91.5%	53.1%	13.5%
	Al_2O_3	0.2%	43.8%	19.6%	9.6%
	Fe_2O_3	0.2%	31.0%	5.8%	6.5%
	Amorphous phase	18.8%	100%	72.8%	20.8%
Output	Cumulative heat at 7 days (J/g SCM)	76.0	1014.1	339.4	216.4

5 ML-Based Prediction Models for Evaluating the Reactivity

5.1 ML-Based Prediction Models

The accuracy of predicting the cumulative heat release of SCMs-incorporated R^3 paste at 7 days was investigated using LR, ANN, SVM, and RF models. Each prediction model was trained and tested using the same data set. For the LR model, the updated coefficients for each input parameter can be expressed as follows:

$$\begin{aligned} y = &-64.2 - 1.5x_1 - 538.1x_2 \\ &+ 1228.5x_3 - 1619.2x_4 \\ &- 394.8x_5 + 138.3x_6 + 343.0x_7, \end{aligned} \tag{11}$$

where $x_1 \sim x_7$ indicate input parameters of particle size of D50, density, content of CaO, SiO_2, Al_2O_3, Fe_2O_3, and amorphous phase, respectively. The ANN model, comprising 20 neurons in each of the 5 hidden layers, utilized the scaled conjugate gradient backpropagation method for training. The tangent sigmoid transfer function served as the activation function. The SVM model employed the Gaussian kernel function, considering the nonlinearity of input and output variables, with fine-tuned hyperparameters related to box constraint and kernel scale. The RF model, comprising 100 regression trees, used the ensemble aggregation algorithm of least-squares boosting. Since it is a boosting algorithm, the ensemble was composed of regression trees allowing a maximum of 5 splits, and a learning rate of 0.1 was selected.

The results for each prediction model are summarized in Fig. 8 and Table 4. Due to the complex relationship between inputs and cumulative heat release, the LR model exhibited poor prediction accuracy, indicated by a high training MAE of 42.2%, suggesting an underfitting problem. For the ANN model, the training and testing MAEs were 9.2% and 9.6%, respectively. The RF and SVM models exhibited 10.8% and 8.9% training MAEs, respectively. Meanwhile, their testing MAEs were 22.0% and 21.5%, respectively. Consequently, it was observed that the ANN model demonstrated a good performance in predicting the cumulative heat release of R^3 pastes.

With respect to the centered RMSE, r value, and standard deviation, the performance of different prediction models on the testing data was compared using a Taylor diagram, as depicted in Fig. 9. It should be noted that centered RMSE can be obtained using a below equation:

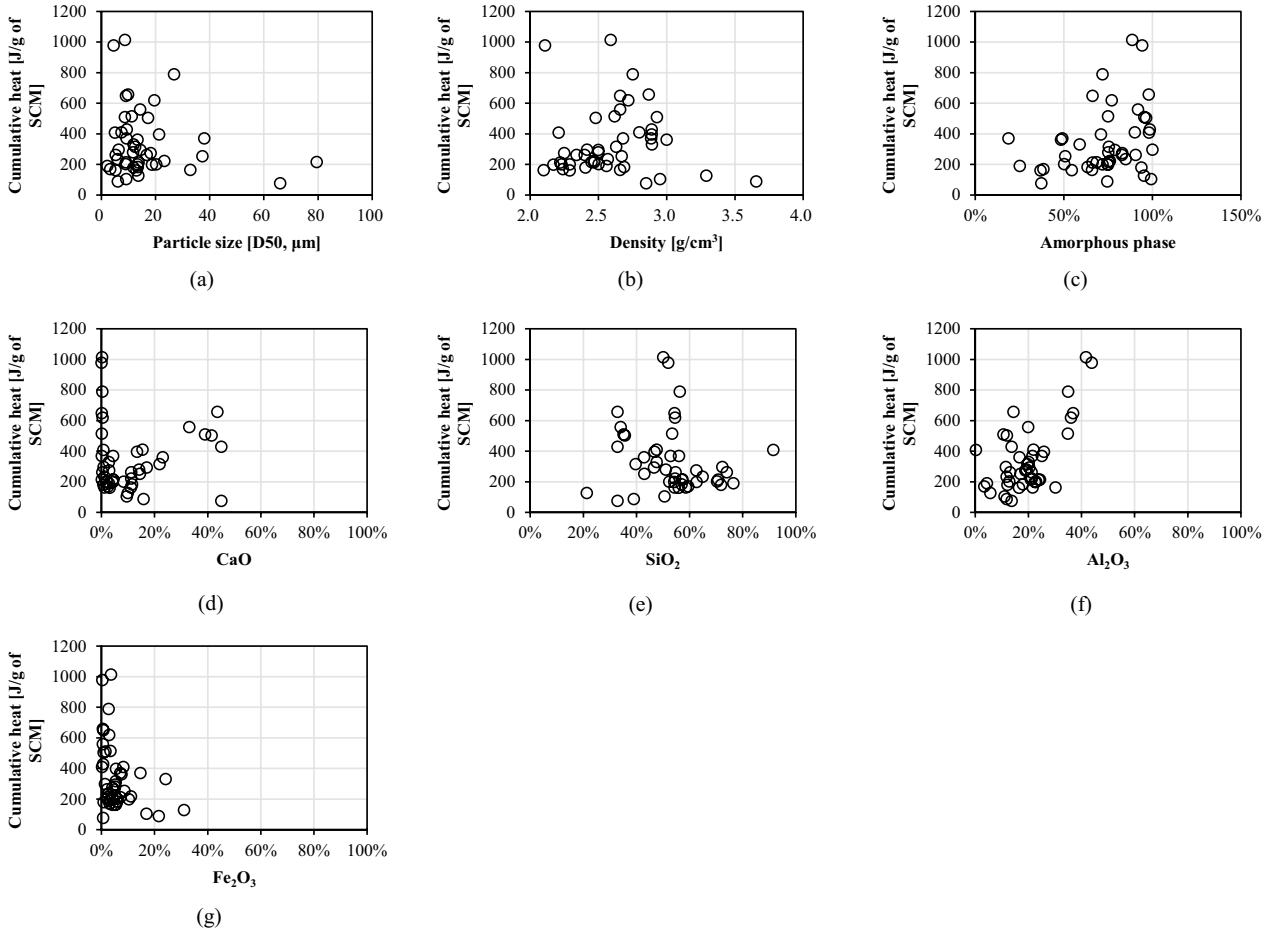

Fig. 7 Correlations of cumulative heat release at 7 days with (**a**) particle size, (**b**) density, (**c**) amorphous phase, (**d**) CaO, (**e**) SiO_2, (**f**) Al_2O_3, and (**g**) Fe_2O_3

$$\text{centered RMSE} = \sqrt{\text{RMSE}^2 - \left(\overline{a} - \overline{b}\right)^2}, \tag{12}$$

where $\overline{a}$ and $\overline{b}$ indicate average of target and prediction from the ML models. In general, ML-based prediction models exhibited superior performance when compared to the LR model. The standard deviation for ANN, RF, and SVM models ranged from 43.1 to 100.6. Among these ML models, the RF model displayed the lowest standard deviation. In terms of centered RMSE, for the ANN model, it achieved the lowest RMSE at 22.5, coupled with the highest r of 0.97, indicative of its robustness and excellent performance. The other ML models, SVM and RF, had centered RMSE values of 100.6 and 63.6, respectively, with correlation coefficients of 0.21 and 0.79. In contrast, the LR model exhibited a higher RMSE of 114.2. These results affirmed that the ANN model demonstrated notable effectiveness and robust performance compared to the other models evaluated.

5.2 Feature Importance

Feature importance analysis is valuable in understanding crucial input parameters for predicting a target, and this can be achieved through the RF model using Eq. (7). As depicted in Fig. 10, the relative importance of each input parameter on cumulative heat release was determined. Notably, Al_2O_3 exhibited a significantly high relative importance compared to other parameters. This prominence can be attributed to the fact that the early-age heat of hydration of cementitious materials and the reaction of SCMs are predominantly influenced by the Al_2O_3 content. This might be attributed that highly reactive SCMs, such as calcined clay, GGBFS, and metakaolin, tended to contained relatively larger amount of Al_2O_3. This estimation corresponded to the results provided in Fig. 7f. A robust linear correlation between cumulative heat release at 7 days and the Al_2O_3 content of SCMs was identified.

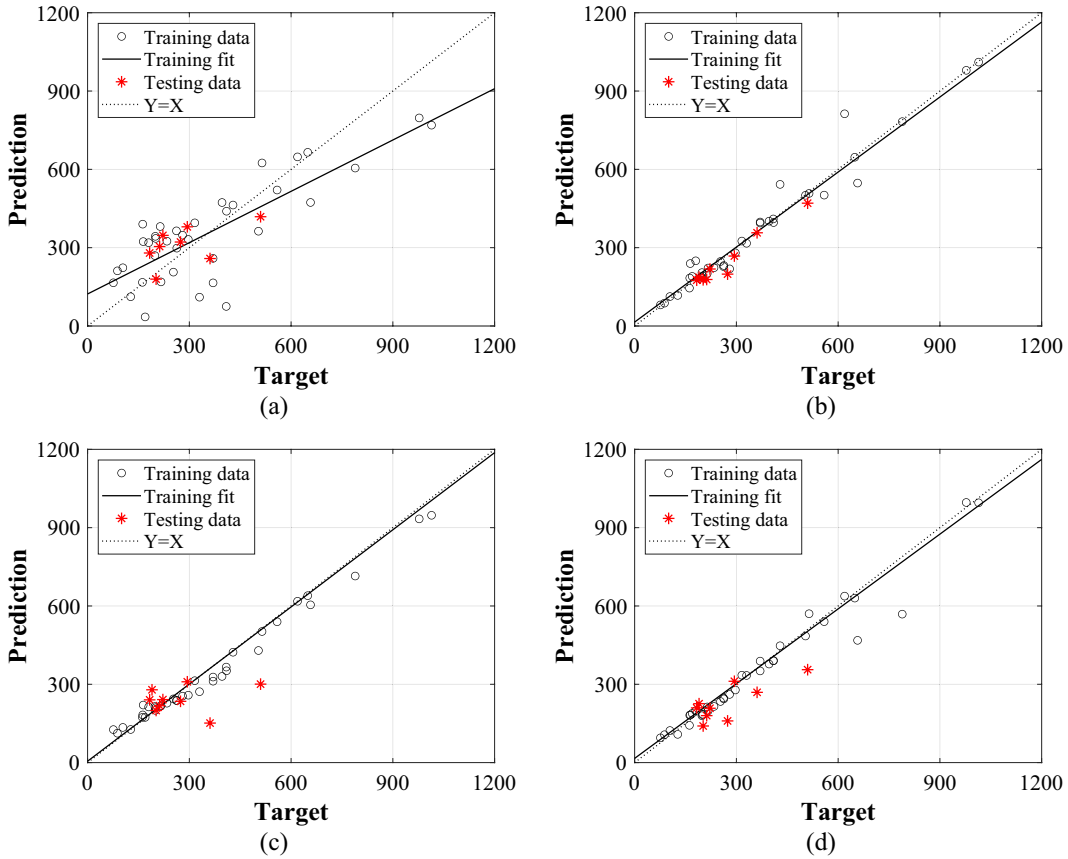

Fig. 8 Prediction results for the R^3-based cumulative heat release at 7 days obtained from (**a**) LR, (**b**) ANN, (**c**) RF, and (**d**) SVM (unit for prediction and target: J/g of SCM)

Table 4 Prediction accuracies in terms of MSE, MAE, and *r*

	Training			Testing		
	MAE (%)	**RMSE**	***r***	**MAE**	**RMSE**	***r***
LR	44.7	135.3	0.81	42.2	114.2	0.53
ANN	9.2	48.4	0.98	9.6	33.4	0.97
RF	10.8	37.4	0.99	22.0	106.8	0.21
SVM	8.9	51.6	0.98	21.5	82.1	0.79

6 Discussion

In Sect. 5, it was determined that the ANN model exhibited the highest prediction accuracies, boasting training and testing MAEs of 9.2% and 9.6%, respectively. The results for all 46 data points are depicted in Fig. 11. On the whole, the target and prediction outcomes from the ANN model displayed acceptable correspondence. This indicates that various types of SCMs exhibited satisfactory agreement in predictions, even in the presence of notable variations in their material properties.

To assess the effect of various types of SCMs on reactivity, as indicated by cumulative heat release at 7 days, a comparison of ANN-based prediction results based on SCM types was conducted. For a comprehensive analysis, material properties in terms of D50, density, amorphous phase, SiO_2, Al_2O_3, Fe_2O_3, CaO were normalized in a range of 0 to 1 using the min–max normalization equation as follows (Yoon et al. 2023):

$$x_{\text{nor}} = \frac{x - x_{\text{min}}}{x_{\text{max}} - x_{\text{min}}}. \tag{13}$$

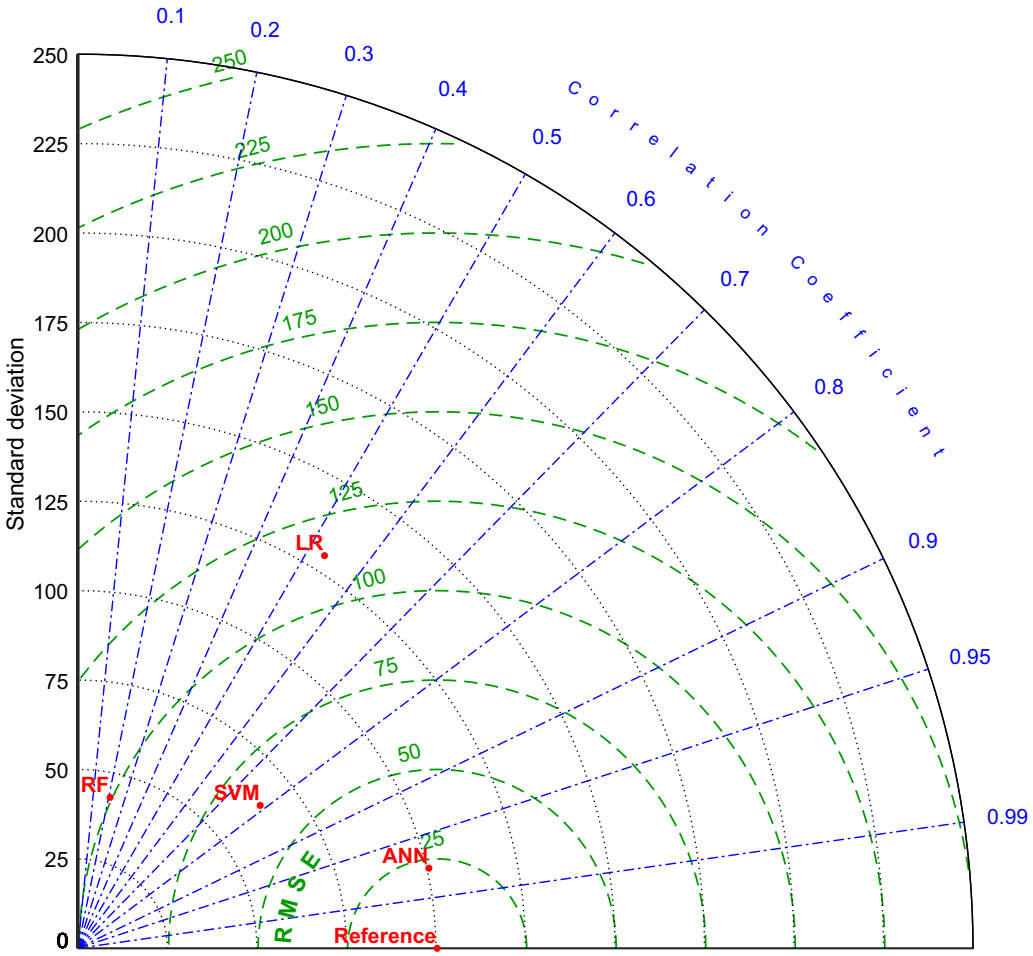

Fig. 9 Taylor diagram for a comparative analysis on LR, ANN, RF, and SVM models

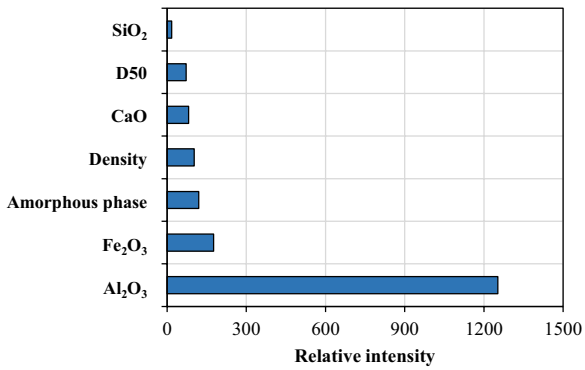

Fig. 10 Feature importance of input parameters obtained from the RF model

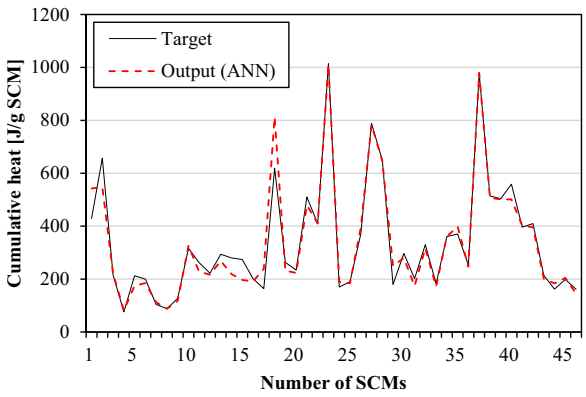

Fig. 11 Prediction results for cumulative heat release at 7 days using the ANN model

Substantial variations in physical and chemical properties were observed for SCMs in the same category, such as CC, Class F FA, BA, and metakaolin as shown in Fig. 12a–c, and e. However, despite these differences, they exhibited good linear correlations with a R^2 higher than 0.90 due to the excellent robustness of the ANN

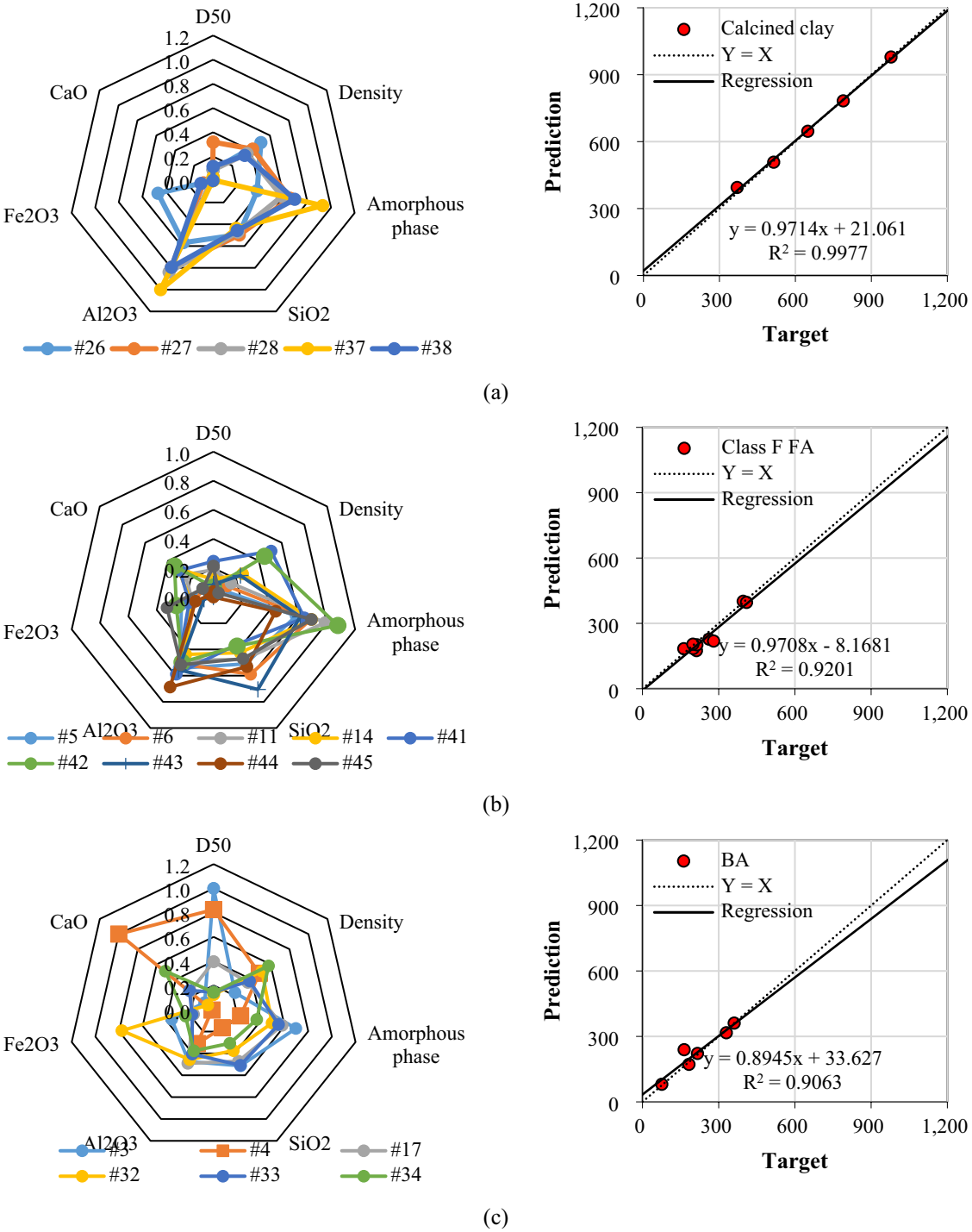

Fig. 12 Variations in material properties (left) for each type of SCM and evaluation of ANN-based prediction accuracies in terms of cumulative heat release at 7 days (right): (**a**) calcined clay, (**b**) Class F fly ash, (**c**) ground bottom ash, (**d**) ground granulated blast furnace slag (GGBFS), (**e**) metakaolin, and (**f**) other SCMs (e.g., volcanic ash, silica fume, fluidized bed combustion ash, blended SCMs, etc.)

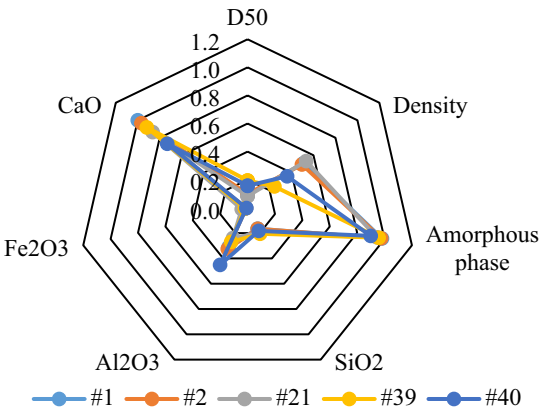

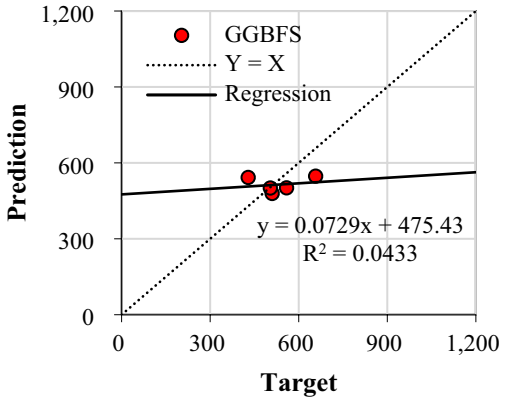

(d)

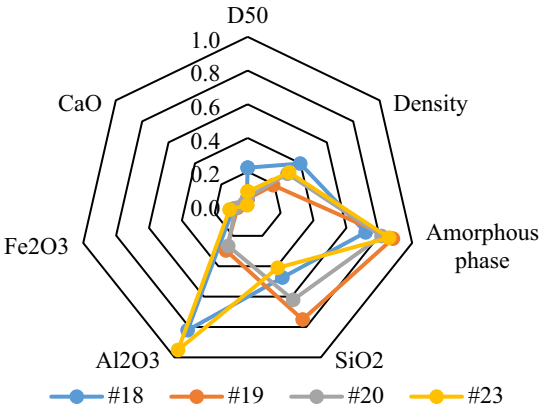

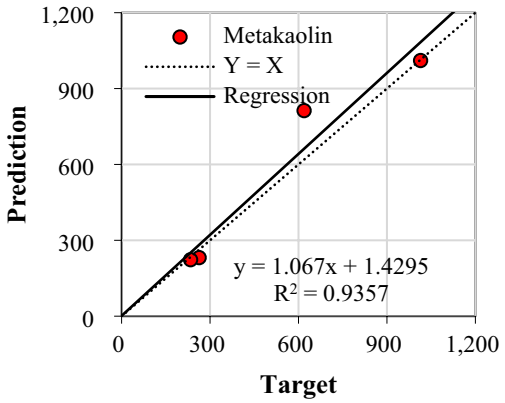

(e)

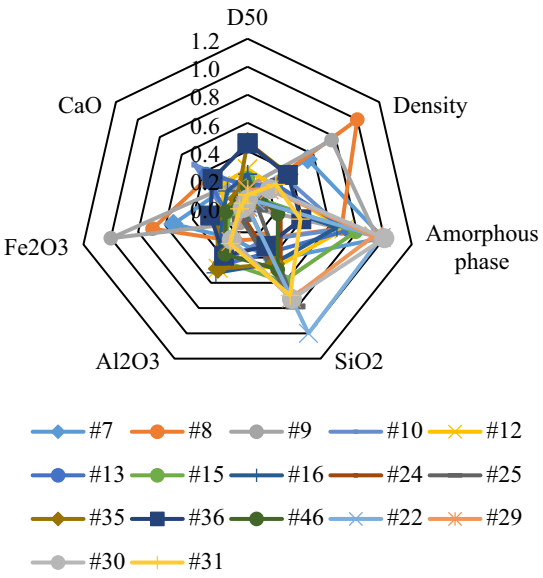

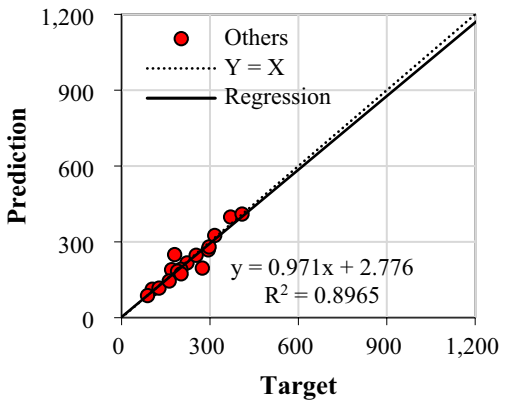

(f)

Fig. 12 continued

Table 5 Characteristics of GGBFS in terms of material properties and 7-day cumulative heat release from the R^3 test

GGBFS	D50 (μm)	Density (g/cm^3)	Amorphous phase (%)	SiO_2 (%)	Al_2O_3 (%)	Fe_2O_3 (%)	CaO (%)	Cumulative heat release at 7 days (J/g of SCM)	
								Target	Output (ANN)
#1	9.3	2.89	98.5	32.9	13.7	0.6	45.1	428.8	542.4
#2	9.8	2.87	98.0	33.0	14.4	0.5	43.6	657.3	547.5
#21	8.6	2.93	95.5	35.2	10.6	1.5	39.0	510.0	479.1
#39	17.2	2.48	96.5	35.7	11.9	0.8	41.4	503.8	500.7
#40	14.3	2.66	91.8	34.1	19.9	0.5	33.0	558.8	501.3

model and quality of the database. In case of GGBFS, a good agreement between the target and prediction results was also observed. However, its R^2 value was as low as 0.04 due to closely located data points. This could be attributed to slightly different cumulative heat release values despite very similar physical and chemical properties of GGBFS (see Table 5). To precisely estimate the reactivity of GGBFS, incorporating additional relevant input parameters, such as fineness, LOI, carbon content, and other chemical compositions (MgO, K_2O, Na_2O, etc.) might be needed (Blotevogel et al. 2020; Zhu et al. 2020).

7 Conclusion

In this study, an extensive exploration of the relationship between material properties and the reactivity of various SCMs was undertaken using ML models. The investigation encompassed six SCMs, including GGBFS, FA, and BA, with a focus on their physical and chemical properties. Experimental identification material characteristics and reactivity tests, including the modified SAI and R^3 test were conducted. A total of 46 database, obtained through experimental results and literature review, were utilized for training ML models, such as ANN, SVM, and RF. The ANN model exhibited favorable prediction results, leading to the following conclusions.

- Commonly used SCMs of GGBFS and FA and non-conventional SCMs of BA were used for material characterization and reactivity test. Reactivity test included the modified SAI and R^3 test in terms of the bound water and cumulative heat release. Good correlations were observed between the results of the modified SAI and R^3 test. Based on this, reactivity of SCMs can be classified into good (GS1 and GS2), moderate (BA1, FA1, and FA2), and low (BA2) reactivities.
- A comprehensive database integrating material properties and R^3-based reactivity was established, combining experimental results and literature data. Critical input parameters, including particle size of D50, density, chemical composition of SiO_2, Al_2O_3, Fe_2O_3, and CaO, and amorphous phase were selected based on their correlations with reactivity. This data set, comprising 46 entries, served as the foundation for ML model training.
- The ANN model demonstrated the highest prediction accuracies, achieving a testing MAE of 13.5% compared to SVM and RF models. Further investigation into prediction results considering different SCM types revealed a generally high level of agreement. Notably, GGBFS, despite having similar material properties, exhibited slightly differences in R^3-based heat release. Recommendations were made to enhance accuracy for GGBFS by incorporating additional input parameters, such as fineness.

In summary, this study contributes valuable insights into predicting SCM reactivity, emphasizing the efficacy of ML models, particularly the ANN model, for informed material selection and optimization in concrete applications. The findings underscore the importance of comprehensive databases and considerations of specific input parameters for accurate predictions, setting the stage for further advancements in SCM reactivity modeling.

Appendix

See Table 6.

Table 6 Summary of data set

Reference	Materials	Label	PSD D50 (μm)	Density	Amorphous phase (%)	SiO_2 (%)	Al_2O_3 (%)	Fe_2O_3 (%)	CaO (%)	Heat release (R^3 test)		SAI (relative strength) (%)	
										3 days (J/g SCM)	7 days (J/g SCM)	7 days	28 days
Experimental results	Ground granulated blast furnace slag	#1 GS1	9.3	2.89	98.5	32.9	13.7	0.6	45.1	661.3	714.7	70.5	113.4
	Ground granulated blast furnace slag	#2 GS2	9.8	2.87	98.0	33.0	14.4	0.5	43.6	838.7	1102.1	100.8	123.3
	Ground bottom ash	#3 BA1	79.5	2.45	66.2	57.1	23.9	7.1	4.3	202.3	324.1	57.3	73.1
	Ground bottom ash	#4 BA2	66.0	2.85	74.6	62.7	22.5	4.2	4.2	208.6	351.1	58.6	69.0
	Fly ash	#5 FA1	13.7	2.22	75.2	57.3	20.9	11.1	4.3	169.3	373.9	71.9	83.1
	Fly ash	#6 FA2	13.3	2.29	37.3	32.9	13.7	0.6	45.1	116.5	133.6	59.1	68.5
Vayghan et al. (2021)	Non-ferrous metallurgical slags treated at 1200°C for 4 h	#7 TS1	9.1	2.95	99.2	50.6	11.0	16.9	9.5	58.0	104.0	–	–
	Non-ferrous metallurgical slags treated at 1200°C for 2 h	#8 TS2	6.0	3.66	74.5	39.0	11.8	21.6	15.8	58.0	88.0	–	–
	Non-ferrous metallurgical slags treated at 1200°C for 3.5 h	#9 TS3	13.6	3.29	95.3	21.3	5.7	31.0	9.9	73.0	127.0	–	–

Table 6 (continued)

Reference	Materials	Label	PSD D50 (μm)	Density	Amorphous phase (%)	SiO_2 (%)	Al_2O_3 (%)	Fe_2O_3 (%)	CaO (%)	Heat release (R^3 test)		SAI (relative strength) (%)	
										3 days (J/g SCM)	7 days (J/g SCM)	7 days	28 days
Al-Shmaisani et al. (2022)	Class C fly ash	#10 CA	12.4	2.63	75.4	39.7	19.6	5.3	21.9	–	316.0	89.2	108.8
	Class F fly ash	#11 FA	16.7	2.34	82.8	54.8	21.2	4.7	11.2	–	262.0	77.4	86.9
	Blended, class F and ground bottom ash	#12 FBA	23.2	2.47	76.0	54.6	21.3	5.0	11.2	–	222.0	65.5	82.0
	Blended, class F and class C	#13 FC	14.4	2.50	78.8	46.6	20.3	5.1	17.0	–	294.0	79.6	97.6
	Class F fly ash and powder River Basin coal blends	#14 FLP	11.6	2.50	75.1	51.1	19.3	5.0	14.1	–	280.0	75.0	92.4
	Class F fly ash remediated by blending with class N natural Pozzolan	#15 FR-N	18.1	2.25	83.0	62.6	18.8	4.1	2.9	–	274.0	78.9	95.2
	Class F fly ash remediated by treating for SO_3 content	#16 FR-S	20.2	2.23	71.8	52.4	22.9	5.7	8.3	–	201.0	89.5	102.0
	Milled bottom ash	#17 MBA	32.8	2.66	65.9	54.4	21.6	5.4	11.1	–	164.0	66.0	78.3
	Impure metakaolin	#18 MI	19.5	2.72	77.0	54.6	36.0	2.9	0.4	–	619.0	91.0	113.5
	Metakaolin (pure pumicite)	#19 PP	5.2	2.40	90.5	74.0	13.1	2.1	0.3	–	263.0	80.9	98.3
	Impure pumicite	#20 PI	5.9	2.57	84.9	64.9	11.8	2.5	1.1	–	234.0	83.3	101.2
	Slag (grade100)	#21 S	8.6	2.93	95.5	35.2	10.6	1.5	39.0	–	510.0	94.5	116.1

Table 6 (continued)

Reference	Materials	Label	PSD D50 (μm)	Density	Amorphous phase (%)	SiO_2 (%)	Al_2O_3 (%)	Fe_2O_3 (%)	CaO (%)	Heat release (R^3 test)		SAI (relative strength) (%)	
										3 days (J/g SCM)	7 days (J/g SCM)	7 days	28 days
de Azevedo Basto et al. (2023)	Silica fume	#22 SF	5.0	2.21	98.1	91.5	0.2	0.2	0.7	335.1	408.8	86.2	106.8
	Metakaolin	#23 MK	8.6	2.59	88.6	50.1	41.7	3.6	0.2	981.6	1014.1	85.9	103.0
	Boiler ash: sugar-cane bagasse ashes	#24 SCBA	3.2	2.24	38.4	59.5	3.4	3.1	2.5	123.6	169.7	64.5	85.8
	Ground SCBA	#25 SCBA600	2.2	2.56	25.1	76.5	4.4	3.0	2.8	136.1	189.9	71.3	96.6
Yoon et al. (2022)	Calcined clay	#26 CC1	9.2	2.89	49.1	56.0	25.0	14.6	0.1	347	370.0	96.3	89.3
	Calcined clay	#27 CC2	26.8	2.75	71.9	56.3	34.9	2.7	0.3	523.2	789.0	94.4	91.9
	Calcined clay	#28 CC3	9.0	2.66	66.2	54.4	36.8	0.7	0.1	595.6	649.0	103.4	95.0
	Volcanic ash	#29 VA1	11.8	2.41	93.8	71.9	12.1	0.8	0.7	142.9	180.0	93.8	105.9
	Volcanic ash	#30 VA2	6.3	2.42	100.0	72.4	11.5	1.3	0.8	191.8	297.0	87.8	105.9
	Volcanic ash	#31 VA3	8.9	2.50	50.2	70.4	12.8	2.0	1.9	136.7	202.0	91.8	107.1
	Ground bottom ash	#32 GBA1	11.8	2.89	58.9	47.6	20.1	24.1	2.8	194.0	330.0	88.4	87.4
	Ground bottom ash	#33 GBA2	13.4	2.69	63.4	57.0	17.9	5.8	11.5	200.1	183.0	85.8	81.7
	Ground bottom ash	#34 GBA3	13.3	3.00	48.4	42.9	16.6	7.5	23.0	151.5	361.0	89.1	96.0
	Fluidized bed combustion ash	#35 FBC1	37.9	2.68	18.8	52.9	21.5	7.0	4.3	140.8	370.0	87.6	86.1
	Fluidized bed combustion ash	#36 FBC2	37.3	2.67	50.7	43.0	17.0	8.6	14.4	199.6	253.0	85.5	91.3

Table 6 (continued)

Reference	Materials	Label	PSD D50 (μm)	Density	Amorphous phase (%)	SiO_2 (%)	Al_2O_3 (%)	Fe_2O_3 (%)	CaO (%)	Heat release (R^3 test)		SAI (relative strength) (%)	
										3 days (J/g SCM)	7 days (J/g SCM)	7 days	28 days
Li et al. (2018)	Calcined clay	#37 CC1	4.5	2.11	94.2	52.0	43.8	0.3	0.0	947.3	977.7	–	121.3
	Calcined clay	#38 CC2	11.2	2.62	75.0	53.5	34.9	3.4	0.1	476.8	514.3	–	97.4
	Ground granulated blast furnace slag	#39 S1	17.2	2.48	96.5	35.7	11.9	0.8	41.4	432.4	503.8	–	102.1
	Ground granulated blast furnace slag	#40 S8	14.3	2.66	91.8	34.1	19.9	0.5	33.0	454.1	558.8	–	103.4
	Fly ash	#41 CFA-P	21.2	2.89	70.9	46.8	25.9	5.5	13.4	310.0	396.4	–	89.1
	Fly ash	#42 CFA-S	7.4	2.80	90.1	47.6	21.9	8.3	15.5	272.1	409.6	–	94.6
	Fly ash	#43 SFA-E	9.0	2.47	68.5	70.8	24.4	2.2	0.1	119.6	214.1	–	84.1
	Fly ash	#44 SFA-I	5.1	2.10	54.5	58.6	30.2	4.1	1.1	81.6	162.5	–	77.3
	Fly ash	#45 SFA-R	18.6	2.17	75.0	54.3	22.7	10.3	4.3	113.2	198.4	–	76.9
	Natural Pozzolan	#46 P0	12.9	2.29	36.8	56.0	16.5	5.1	3.0	116.7	161.6	–	85.8

Acknowledgements
This work was supported by Konkuk University in 2024 (Project number: 2024-A019-0005).

Author contributions
Jinyoung Yoon: conceptualization, writing—original draft, writing—review and editing, supervision, project administration; Aidarus Yonis: formal analysis, data curation, methodology; Sungwoo Park: writing—review and editing; Farshad Rajabipour: writing—review and editing, and supervision; Sukhoon Pyo: writing—review and editing, and supervision.

Availability of data and materials
The data and materials are included in the manuscript.

Declarations

Ethics approval and consent to participate
Not applicable.

Consent for publication
Not applicable.

Competing interests
The authors declare that they have no known competing financial interests or personal relationships that could have appeared to influence the work reported in this paper.

Received: 10 June 2024 Accepted: 5 August 2024
Published online: 01 November 2024

References

Al-Shmaisani, S., Kalina, R. D., Ferron, R. D., & Juenger, M. C. G. (2022). Comparison of SCM reactivity to performance in cement-based mixtures. *Materials and Structures, 55*(10), 1–20. https://doi.org/10.1617/S11527-022-02072-X/FIGURES/8

ASTM C188-17, Standard test method for density of hydraulic cement (2017).

ASTM C311/C311M-18, Standard test methods for sampling and testing fly ash or natural Pozzolans for use in portland-cement concrete (2018).

ASTM C618-19, Standard specification for coal fly ash and raw or calcined natural Pozzolan for use in concrete (2019).

ASTM C1897-20, Standard test methods for measuring the reactivity of supplementary cementitious materials by isothermal calorimetry and bound water measurements (2020).

Avet, F., Li, X., Ben Haha, M., Bernal, S. A., Bishnoi, S., Cizer, Ö., et al. (2022). Report of RILEM TC 267-TRM phase 2: Optimization and testing of the robustness of the R3 reactivity tests for supplementary cementitious materials. *Materials and Structures, 55*(3), 1–14. https://doi.org/10.1617/S11527-022-01928-6/TABLES/6

Avet, F., Snellings, R., Alujas Diaz, A., Ben Haha, M., & Scrivener, K. (2016). Development of a new rapid, relevant and reliable (R3) test method to evaluate the pozzolanic reactivity of calcined kaolinitic clays. *Cement and Concrete Research, 85*, 1–11. https://doi.org/10.1016/j.cemconres.2016.02.015

Blotevogel, S., Ehrenberg, A., Steger, L., Doussang, L., Kaknics, J., Patapy, C., & Cyr, M. (2020). Ability of the R3 test to evaluate differences in early age reactivity of 16 industrial ground granulated blast furnace slags (GGBS). *Cement and Concrete Research, 130*, 105998. https://doi.org/10.1016/J.CEMCONRES.2020.105998

Breiman, L. (2001). Random forests. *Machine Learning*.

Cortes, C., & Vapnik, V. (1995). Support-vector networks. *Machine Learning., 20*, 237.

de Azevedo Basto, P., Estolano de Lima, V., & de Melo Neto, A. (2023). Capability of R3 test to evaluate pozzolanicity of ground raw and calcined sugarcane bagasse ashes. *Materials Today Proceedings*. https://doi.org/10.1016/J.MATPR.2023.04.048

de Chapelle, J. (1958). Attaque sulfocalcique des laitiers et pouzzolanes. *Revue Des Materiaux De Construction, 512*, 136–145.

Dhandapani, Y., Santhanam, M., Kaladharan, G., & Ramanathan, S. (2021). Towards ternary binders involving limestone additions—A review. *Cement and Concrete Research, 143*, 106396. https://doi.org/10.1016/J.CEMCONRES.2021.106396

Donatello, S., Tyrer, M., & Cheeseman, C. R. (2010). Comparison of test methods to assess pozzolanic activity. *Cement and Concrete Composites, 32*(2), 121–127. https://doi.org/10.1016/j.cemconcomp.2009.10.008

EN 196-5. Standard methods for testing cement. Part 5: Pozzolanicity test for pozzolanic cements (1988).

Eskandari-Naddaf, H., & Kazemi, R. (2017). ANN prediction of cement mortar compressive strength, influence of cement strength class. *Construction and Building Materials, 138*, 1–11.

Flegar, M., Serdar, M., Londono-Zuluaga, D., & Scrivener, K. (2020). Regional waste streams as potential raw materials for immediate implementation in cement production. *Materials, 13*(23), 5456. https://doi.org/10.3390/MA13235456

Frattini, N. (1949). Richerche sulla calce di idrolisi nelle paste di cimento. *Annali di Chimica*.

Han, Q., Gui, C., Xu, J., & Lacidogna, G. (2019). A generalized method to predict the compressive strength of high-performance concrete by improved random forest algorithm. *Construction and Building Materials, 226*, 734–742. https://doi.org/10.1016/J.CONBUILDMAT.2019.07.315

Inorganic Chemistry Structure Databases (ICSD). (2012). https://icsd.products.fiz-karlsruhe.de/

Jafari, K., Yoon, J., Tokpatayeva, R., Olek, J., & Rajabipour, F. (2022). Surfactant-assisted purification of an impure kaolinite clay to improve its pozzolanic reactivity in concrete. *Journal of Materials in Civil Engineering, 34*(6), 04022094. https://doi.org/10.1061/(ASCE)MT.1943-5533.0004216

Kaladharan, G., Ghantous, R. M., & Rajabipour, F. (2023). Early age hydration behavior of portland cement-based binders incorporating fly ash contaminated with flue gas desulfurization products. *Cement and Concrete Composites, 139*, 105062. https://doi.org/10.1016/J.CEMCONCOMP.2023.105062

Kasaniya, M., Alaibani, A., Thomas, M. D. A., & Riding, K. A. (2022). Exploring the efficacy of emerging reactivity tests in screening pozzolanic materials. *Construction and Building Materials, 325*, 126781. https://doi.org/10.1016/J.CONBUILDMAT.2022.126781

Kim, H. K. (2015). Utilization of sieved and ground coal bottom ash powders as a coarse binder in high-strength mortar to improve workability. *Construction and Building Materials, 91*, 57–64. https://doi.org/10.1016/j.conbuildmat.2015.05.017

Kim, Y. H., Kim, H. Y., Yang, K. H., & Ha, J. S. (2021). Effect of concrete unit weight on the mechanical properties of bottom ash aggregate concrete. *Construction and Building Materials, 273*, 121998. https://doi.org/10.1016/J.CONBUILDMAT.2020.121998

Lee, J. Y., Choi, J. S., Yuan, T. F., Yoon, Y. S., & Mitchell, D. (2019). Comparing properties of concrete containing electric arc furnace slag and granulated blast furnace slag. *Materials, 12*(9), 1371. https://doi.org/10.3390/MA12091371

Li, X., Snellings, R., Antoni, M., Alderete, N. M., Ben Haha, M., Bishnoi, S., et al. (2018). Reactivity tests for supplementary cementitious materials: RILEM TC 267-TRM phase 1. *Materials and Structures, 51*(6), 1–14. https://doi.org/10.1617/S11527-018-1269-X/TABLES/5

Li, Z., Yoon, J., Zhang, R., Rajabipour, F., Srubar, W. V., Dabo, I., & Radlińska, A. (2022). Machine learning in concrete science: applications, challenges, and best practices. *NPJ Computational Materials, 8*(1), 1–17. https://doi.org/10.1038/s41524-022-00810-x

Londono-Zuluaga, D., Gholizadeh-Vayghan, A., Winnefeld, F., Avet, F., Ben Haha, M., Bernal, S. A., et al. (2022). Report of RILEM TC 267-TRM phase 3: Validation of the R3 reactivity test across a wide range of materials. *Materials and Structures, 55*(5), 1–16. https://doi.org/10.1617/S11527-022-01947-3/FIGURES/10

Mehta, P. K., & Monteiro, P. J. M. (2013). *Concrete: Microstructure, properties, and materials*. McGraw Hill Professional.

PANalytical X'Pert HighScore Plus [Computer software], Lelyweg, Almelo, the Netherlands.

Parashar, A., & Bishnoi, S. (2020). A comparison of test methods to assess the strength potential of plain and blended supplementary cementitious materials. *Construction and Building Materials, 256*, 119292. https://doi.org/10.1016/J.CONBUILDMAT.2020.119292

Parashar, A., Medepalli, S., & Bishnoi, S. (2023). Reactivity assessment of supplementary cementitious materials and their binary blends using R3 test. *Journal of Materials in Civil Engineering, 35*(2), 04022434. https://doi.org/10.1061/(ASCE)MT.1943-5533.0004607

Pormmoon, P., Abdulmatin, A., Charoenwaiyachet, C., Tangchirapat, W., & Jaturapitakkul, C. (2021). Effect of cut-size particles on the pozzolanic property of bottom ash. *Journal of Materials Research and Technology, 10*, 240–249. https://doi.org/10.1016/J.JMRT.2020.12.017

Scarlett, N. V. Y., & Madsen, I. C. (2006). Quantification of phases with partial or no known crystal structures. *Powder Diffraction, 21*(4), 278–284. https://doi.org/10.1154/1.2362855

Shiuly, A., Hazra, T., Sau, D., & Maji, D. (2022). Performance and optimisation study of waste plastic aggregate based sustainable concrete—A machine learning approach. *Cleaner Waste Systems, 2*, 100014. https://doi.org/10.1016/J.CLWAS.2022.100014

Singh, G. V. P. B., Asce, S. M., Subramaniam, K. V. L., & Asce, M. (2016). Quantitative XRD analysis of binary blends of siliceous fly ash and hydrated cement. *Journal of Materials in Civil Engineering, 28*(8), 04016042. https://doi.org/10.1061/(ASCE)MT.1943-5533.0001554

Sivakumar, P. P., Matthys, S., De Belie, N., & Gruyaert, E. (2021). Reactivity assessment of modified ferro silicate slag by R3 method. *Applied Sciences, 11*(1), 366. https://doi.org/10.3390/APP11010366

Tironi, A., Trezza, M. A., Scian, A. N., & Irassar, E. F. (2013). Assessment of pozzolanic activity of different calcined clays. *Cement and Concrete Composites, 37*(1), 319–327. https://doi.org/10.1016/j.cemconcomp.2013.01.002

Vashistha, P., Oinam, Y., Kim, H. K., & Pyo, S. (2023). Effect of thermo-mechanical activation of waste concrete powder (WCP) on the characteristics of cement mixtures. *Construction and Building Materials, 362*, 129713. https://doi.org/10.1016/J.CONBUILDMAT.2022.129713

Vayghan, A. G., Horckmans, L., Snellings, R., Peys, A., Teck, P., Maier, J., et al. (2021). Use of treated non-ferrous metallurgical slags as supplementary cementitious materials in cementitious mixtures. *Applied Sciences, 11*(9), 4028. https://doi.org/10.3390/APP11094028

Vladić Kancir, I., & Serdar, M. (2022). Contribution to understanding of synergy between red mud and common supplementary cementitious materials. *Materials, 15*(5), 1968. https://doi.org/10.3390/MA15051968

Walker, R., & Pavía, S. (2011). Physical properties and reactivity of pozzolans, and their influence on the properties of lime-pozzolan pastes. *Materials and Structures, 44*(6), 1139–1150. https://doi.org/10.1617/S11527-010-9689-2/FIGURES/8

Wang, Y. (2023). *Reactivity and reactivity tests for unconventional fly ashes*. University of Miami.

Wang, Y., Burris, L., Shearer, C. R., Hooton, D., & Suraneni, P. (2021). Strength activity index and bulk resistivity index modifications that differentiate inert and reactive materials. *Cement and Concrete Composites, 124*, 104240. https://doi.org/10.1016/J.CEMCONCOMP.2021.104240

Weise, K., Ukrainczyk, N., & Koenders, E. (2021). A mass balance approach for thermogravimetric analysis in pozzolanic reactivity R3 test and effect of drying methods. *Materials, 14*(19), 5859. https://doi.org/10.3390/MA14195859

Yoon, J., Jafari, K., Tokpatayeva, R., Peethamparan, S., Olek, J., & Rajabipour, F. (2022). Characterization and quantification of the pozzolanic reactivity of natural and non-conventional pozzolans. *Cement and Concrete Composites, 133*, 104708. https://doi.org/10.1016/J.CEMCONCOMP.2022.104708

Yoon, J., Kim, H., Ju, S., Li, Z., & Pyo, S. (2023). Framework for rapid characterization of fresh properties of cementitious materials using point cloud and machine learning. *Construction and Building Materials, 400*, 132647. https://doi.org/10.1016/J.CONBUILDMAT.2023.132647

Yoon, J. Y., Kim, H., Lee, Y.-J., & Sim, S.-H. (2019a). Prediction model for mechanical properties of lightweight aggregate concrete using artificial neural network. *Materials, 12*(17), 2678.

Yoon, J. Y., Lee, J. Y., & Kim, J. H. (2019b). Use of raw-state bottom ash for aggregates in construction materials. *Journal of Material Cycles and Waste Management, 21*, 1–12. https://doi.org/10.1007/s10163-019-00841-5

Yu, Y., Li, W., Li, J., & Nguyen, T. N. (2018). A novel optimised self-learning method for compressive strength prediction of high performance concrete. *Construction and Building Materials, 184*, 229–247.

Zhu, X., Zhang, M., Yang, K., Yu, L., & Yang, C. (2020). Setting behaviours and early-age microstructures of alkali-activated ground granulated blast furnace slag (GGBS) from different regions in China. *Cement and Concrete Composites, 114*, 103782. https://doi.org/10.1016/J.CEMCONCOMP.2020.103782

Publisher's Note

Springer Nature remains neutral with regard to jurisdictional claims in published maps and institutional affiliations.

Jinyoung Yoon Assistant Professor in the Department of Civil and Environmental Engineering at Konkuk University, Seoul, Republic of Korea.

Aidarus Yonis Master's student in the Department of Civil, Urban, Earth, and Environmental Engineering at Ulsan National Institute of Science and Technology (UNIST), Ulsan, Republic of Korea.

Sungwoo Park Assistant Professor in the School of Architecture and Building Science at Chung-Ang University, Seoul, Republic of Korea.

Farshad Rajabipour Professor and Interim Head of the Department of Civil and Environmental Engineering at Pennsylvania State University, University Park, PA, United States.

Sukhoon Pyo Associate Professor in the Department of Civil, Urban, Earth, and Environmental Engineering at Ulsan National Institute of Science and Technology (UNIST), Ulsan, Republic of Korea.